Evaluation of cloud thermodynamic phase parametrizations in the LMDZ GCM by using POLDER satellite data

M. Doutriaux-Boucher
Laboratoire d'Optique Atmosphérique, USTL/CNRS, Villeneuve d'Ascq, France

J. Quaas
Laboratoire de Météorologie Dynamique, IPSL/CNRS, Paris, France

Received 18 November 2003; revised 20 January 2004; accepted 20 February 2004; published 30 March 2004.

[1] Realistic simulations of clouds are of uppermost importance for climate modelling using general circulation models. Satellite data are well suited to evaluate model parametrizations. In this study we use the Laboratoire de Météorologie Dynamique general circulation model (LMDZ). We evaluate the current LMDZ cloud phase parametrization, in which the repartition of condensed cloud water between liquid and ice is a function of the local temperature. Three parameters are used to derive a relation between liquid cloud water content and temperature, two of which are not physically based. We use the POLDER-1 satellite data to infer more realistic parameters by establishing statistical relationships between cloud top thermodynamical phase and cloud top temperature, consistently in both satellite data and model results. We then perform a multitude of short model integrations and derive a best estimate for the lowest local temperature where liquid water can exist in a cloud ($T_{ice} = -32°C$ in our parametrization). The other parameter which describes the shape of the transition between ice and liquid water is also estimated. A longer simulation has then been performed with the new parameters, resulting in an improvement in the representation of the shortwave cloud radiative forcing. *INDEX TERMS:* 0320 Atmospheric Composition and Structure: Cloud physics and chemistry; 0350 Atmospheric Composition and Structure: Pressure, density, and temperature; 3360 Meteorology and Atmospheric Dynamics: Remote sensing. **Citation:** Doutriaux-Boucher, M., and J. Quaas (2004), Evaluation of cloud thermodynamic phase parametrizations in the LMDZ GCM by using POLDER satellite data, *Geophys. Res. Lett.*, *31*, L06126, doi:10.1029/2003GL019095.

1. Introduction

[2] Clouds cover the Earth's surface by about 70% and have a very strong effect on the radiation balance in both the terrestrial and the solar spectrum. Liquid and ice clouds have quite different effects on the Earth radiative balance. Precipitation-forming microphysical processes in ice and mixed-phase clouds are different from those in liquid water clouds. Unfortunately, the representation of clouds in climate models is still unsatisfying. As most cloud properties cannot be resolved by global-scale models, they have to be parameterized in terms of the model variables. Cloud parametrizations are complicated by the fact that clouds cover a large range of scales (from microphysics to mesoscale systems). Moreover they must treat the liquid and ice phases separately. In the absence of explicit liquid and ice cloud microphysics there is no simple parametrizations for the partitioning of condensed water into liquid and ice phase. The local temperature is therefore often used to define the liquid and ice fractions.

[3] Satellites observe clouds with a global coverage at approximately the spatial scale of GCMs. They observe clouds from the top. Various statistical relationships can be inferred between different parameters as seen from satellites. For example, *Tselioudis et al.* [1992] document the optical thickness to temperature relationship for low clouds. Optical thickness increases with increasing temperature for clouds colder than $-10°C$, but decreases with temperature for clouds warmer than $-2°C$. A relationship between cloud-top temperature and cloud-top thermodynamic phase has been established by *Giraud et al.* [2001] using combined data from POLDER-1 and ATSR-2 satellite instruments. They observe a sharp transition between ice and liquid clouds for temperature ranging from 240 to 260 K.

[4] Here we use the data from the POLDER-1 instrument in order to infer a statistical relationship between cloud top temperature and cloud phase and to test the partitioning between liquid and ice water as a function of the local temperature in the atmospheric General Circulation Model (GCM) of the Laboratoire de Météorologie Dynamique (LMD).

2. Tools and Methodology

2.1. POLDER-1 Satellite Observations

[5] POLDER (POLarization and Directionality of the Earth's Reflectances) is a radiometer which was on board the Japanese polar orbiting ADEOS-1 platform from August 1996 until June 1997. POLDER is a wide field-of-view camera (with a swath of 2400×1800 km^2 and a resolution of 6×7 km^2) which observes the Earth's surface and atmosphere through 15 filters and polarizers in the visible and near infrared. It was the first space instrument to simultaneously observe the polarization and the multi-spectral and directional signatures of the reflected radiation [*Deschamp et al.*, 1994]. We use several of the cloud parameters retrieved from POLDER data [*Buriez et al.*, 1997]. The cloud top Rayleigh pressure is retrieved from the polarized signal at 443 nm based on molecular scattering

0094-8276/04/2003GL019095$05.00

by the atmosphere above the cloud [*Vanbauce et al.*, 1998]. The cloud oxygen pressure is derived from the absorption of solar light by O_2 molecules at 763 nm, with a correction for the contribution of the surface [*Vanbauce et al.*, 2003]. Since it is expected that the Rayleigh pressure is closer to the actual cloud top pressure than the oxygen pressure, we only use the former one in this study. Using the corresponding interpolated temperature profile from 6-hourly ECMWF meteorological analyses we convert the cloud top pressure into a cloud top temperature. The cloud top thermodynamic phase is also retrieved from POLDER data as described in *Goloub et al.* [2000] and *Riedi et al.* [2000]. The retrieval is based on the angular and polarized signatures of cloud reflected radiances at scattering angles near 140°.

[6] All these cloud parameters (fraction, pressure, phase) are extracted at the pixel resolution. The POLDER level-2 products are then computed at the scale of "super-pixel" composed of 9 × 9 POLDER level-1 pixels (about 0.5° × 0.5° at the Equator). In POLDER the level-2 cloud phase parameter can take three different values (apart from undetermined): liquid if all cloud pixels are liquid, ice if all cloud pixels are ice, and mixed if both liquid and ice pixels coexist within a super-pixel. The satellite data are used at their original resolution of 9 × 9 pixels as well as at the GCM resolution after an appropriate regridding.

2.2. The LMD GCM

[7] We use here the LMD GCM known as LMDZ. The resolution considered is 96 points evenly spaced in longitude and 72 points in latitude. The model is vertically discretized on 19 hybrid σ-pressure levels ($\sigma = p/p_s$ where p and p_s are the atmospheric and surface pressures, respectively). An important characteristic of the LMD GCM version used in this study is the definition of the cloud and precipitation parametrizations. Cloud water is predicted in the model by a budget equation where the ice and liquid phases are considered jointly. The condensation scheme uses a "hat" probability density function for total water in a grid box, which allows for fractional cloudiness [*Le Treut and Li*, 1991]. Depending on the local temperature, the total condensed water is partitioned between liquid water and ice. Clouds are composed of ice crystals or liquid droplets if the local temperature is lower than T_{ice} and larger than T_0, respectively. In between T_0 and T_{ice}, the fraction of liquid water is given by

$$x_{\text{liq}} = \left(\frac{T - T_{\text{ice}}}{T_0 - T_{\text{ice}}}\right)^{n_x} \tag{1}$$

In the standard version of the model, $T_{\text{ice}} = -15°\text{C}$, $T_0 = 0°\text{C}$, and $n_x = 6$. The choice of $T_0 = 0°\text{C}$ has been made in agreement with most other model parameterizations. Ice crystals in the atmosphere melt rapidly above the melting point so this value represents an upper bound to the presence of ice. The two other parameters, however, do not have a clear physical ground. Their impact on the x_{liq} to T relationship is illustrated in Figure 1. Different values for T_{ice} are found in GCMs: −40°C [*Del Genio et al.*, 1996], −35°C [*Lohmann and Rockner*, 1996], −20°C [*Fowler et al.*, 1996], −15°C [*Smith*, 1990]. Schemes using a formula similar to equation 1 use $n_x = 2$ [*Smith*, 1990].

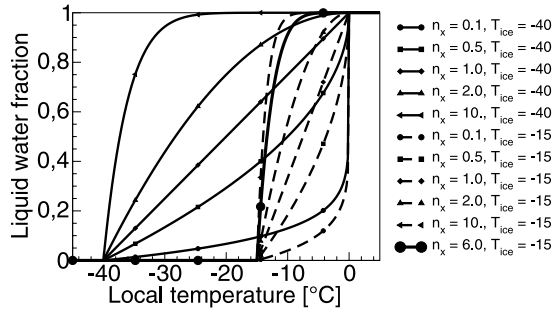

Figure 1. Liquid water fraction as a function of the local temperature for $T_{\text{ice}} = -15°\text{C}$ and $T_{\text{ice}} = -40°\text{C}$, with values for $n_x \in [0.1,0.5,1,2,10]$. The bold line refers to the standard model parameters $T_{\text{ice}} = -15°\text{C}$ and $n_x = 6$.

[8] In this study, we will examine the sensitivity of the model results to these parameters (T_{ice} and n_x) and compare them to the satellite observations. The period simulated is that of POLDER-1 from November 1996 to June 1997. Reynolds sea surface temperature (SST) and HadISST1.0 sea-ice extent [*Rayner et al.*, 2003] are imposed.

2.3. Simulation of Satellite Observations From the Model Results

[9] In order to compare the model results with the satellite parameters, we produce a 2D "satellite-like" field from the 3D model results. For this study, we assume that clouds are opaque for the quantities we are interested in and we use a random overlap assumption (as done in the other model parametrizations). However, the use of random-maximum overlapping assumption give very similar results (not shown). The column cloud fraction, f, can be expressed as:

$$f = 1 - \prod_{i=1}^{n} (1 - f_i)$$

where f_i is the cloud fraction at model layer i and n is the uppermost layer. Under the same assumption the cloudy-sky mean of a variable x (cloud-top temperature, fraction of liquid clouds, ...) as seen from the top of atmosphere can be computed as:

$$x_{\text{cloudy}} = \frac{x_n f_n + (1 - f_n)[x_{n-1} f_{n-1} + (1 - f_{n-1})[\ldots]]}{f} \tag{2}$$

which can also be written as:

$$x_{\text{cloudy}} = \frac{\sum_{i=1}^{n} x_i f_i \prod_{k=i}^{n} (1 - f_{k+1})}{f} \tag{3}$$

using the convention $f_{n+1} = 0$.

[10] For each cloudy layer we approximate the Rayleigh temperature as the temperature of the interface between the cloudy layer and the clear layer above it. We then derive the top-of-atmosphere cloud Rayleigh temperature from equation 3. In the same way a top-of-atmosphere cloud liquid fraction is computed from the cloud liquid fractions at the different levels. Finally the GCM output is sampled along

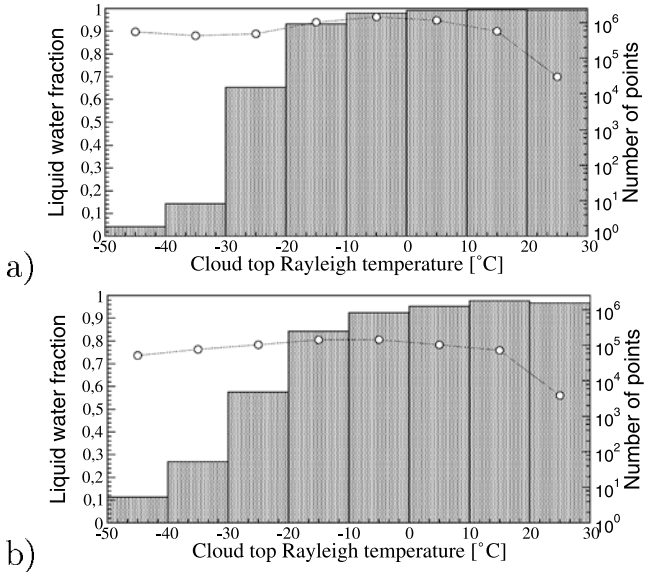

Figure 2. Fraction of liquid water at cloud top as a function of the cloud Rayleigh temperature in the POLDER observations at a) the POLDER resolution and b) the GCM resolution. The dashed line shows the number of points in each bin (right scale).

the satellite overpass which is calculated on-line in the model. Because the physical timestep is 30 minutes in our model, the sampled cloud fields are within ±15 minutes of the actual satellite observations. Therefore we do not expect any bias in the GCM-POLDER comparison due to different sampling of the diurnal cycle.

3. Results

3.1. Cloud Phase to Cloud Temperature Relationship in the Satellite Observations

[11] We first estimate the average liquid cloud fraction for each 10 K bin of cloud Rayleigh temperature in the POLDER retrievals. Figure 2 shows such relationships for the 8-month POLDER period and two different spatial resolutions but relationships for individual months are very similar. It is noteworthy that the relationship is much smoother if POLDER data are regridded to the GCM resolution due to the larger heterogeneity in the cloud properties. Note that due to averaging, we observe a larger liquid (ice) fraction at very low (large) temperatures. It is therefore important to first decrease the resolution of satellite data before comparing with the GCM results.

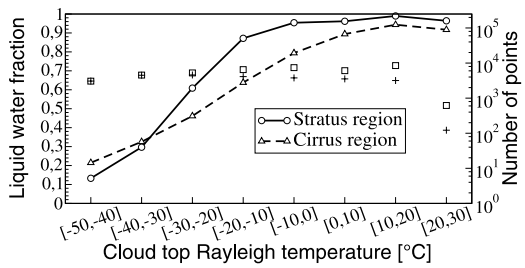

Figure 3. Same as Figure 2b but for the regions of cirrus and stratus clouds. The square and the plus show the number of points in cirrus and stratus regions, respectively.

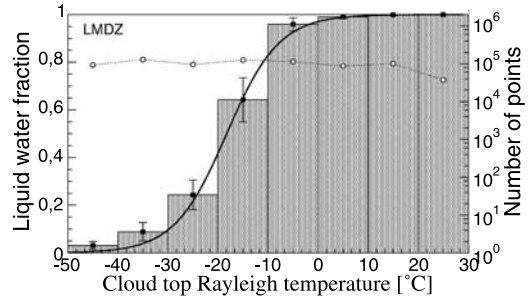

Figure 4. Same as Figure 2b but for standard LMDZ model results.

[12] We also select specific areas which are preferentially covered by cirrus and stratus clouds. Figure 3 shows our cloud liquid fraction to temperature relationships at the GCM resolution for these two regions. The transition between ice and liquid clouds is steeper for stratus clouds than for cirrus clouds. This is expected because of the spatial homogeneity of regions of stratus clouds.

3.2. Model Relationships

[13] Figures 4 and 5 show the same relationships but for model-simulated quantities. An obvious deficiency is the too steep transition between 0% and 100% liquid water fraction in a temperature range of only about 50°C. The model relationship for cirrus and stratus regions is in reasonable agreement with the data although the differences in shape between the two regions is not as pronounced as in the observations.

3.3. Parameter Fit

[14] Keeping the parametrization for the repartition of condensed water into liquid water and ice (equation 1), we try to find the values of the two parameters T_{ice} and n_x which match best the POLDER observations. As shown in Figure 1, we vary T_{ice} between −70°C and 0°C and n_x between 0.1 and 10. We carry out three-day simulations for the period of June 10–12, 1997 for each pair of parameters. It has been verified that results of 3-day simulations are very close to those of longer (month to year) simulations. The resulting dependence of the cloud top liquid water fraction x_{liq} on the cloud top Rayleigh temperature T can be fitted with an hyperbolic tangent function of the form: $x_{liq} = (1 + \tanh(a_1 T + a_2))/2$ with a_1 and a_2 as fitting parameters determining the degree of flatness of the curve and a shift

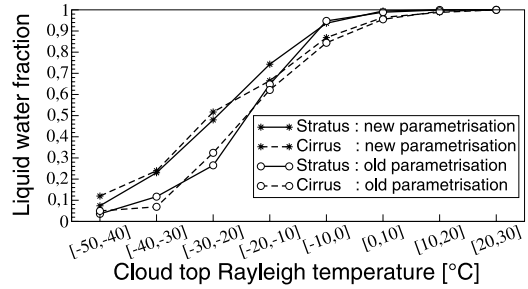

Figure 5. Same as Figure 3 but for the LMDZ model results. Results are shown for the old (standard) and new parametrization.

to lower temperatures, respectively. These functions generally fit very well the relationships.

[15] Figure 6 shows the results of the different simulations in the parameter space of a_1 and a_2. Low T_{ice} temperatures are needed to fit the observations. It needs a rather concave curve ($n_x > 1$) to capture the flat transition between very small liquid water fractions at very low temperatures to larger ones. The best fit in the case examined here would be $T_{ice} = -32°C$ and $n_x = 1.7$. T_{ice} is close to the freezing temperature found by observational studies [*Sassen and Dodd*, 1988]. *Houze* [1993] suggests a range of T_{ice} between $-35°C$ and $-40°C$. This temperature is closer to those used in other GCMs. The n_x value is also closer than those used in other models [*Smith*, 1990].

3.4. Cloud Radiative Forcing

[16] Using these two new values of T_{ice} and n_x, we have run a new one-year simulation. Figure 7 shows the zonal annual mean cloud radiative forcings (CRF) in the short-wave and longwave spectra for the two model versions (old and new parameters). These forcings are compared with ScaRab satellite measurements for March 1994 to February 1995 [*Kandel et al.*, 1998]. New parameters allow a better agreement between observations and simulations in the SW spectrum. The CRF in the LW does not change much and there are some discrepancies at mid- and high latitudes.

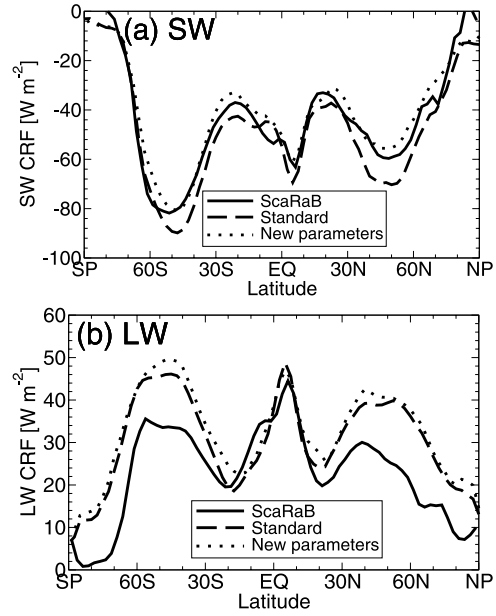

Figure 7. Annually-averaged cloud radiative forcing in the (a) short-wave and (b) long-wave spectrum for ScaRaB observations (solid), the standard model scheme (dashed), and the new pair of parameters (dotted).

4. Conclusion

[17] In the model, the condensed water is partitioned between liquid and ice as a function of the local temperature depending on three parameters (T_{ice}, T_0, and n_x). These parameters are empirical and had to be validated. We use satellite POLDER data to establish a relationship between cloud top temperature and cloud top thermodynamical phase. We interpolate this relationship using a two-parameter (a_1 and a_2) hyperbolic tangent fit to the data. We carried out multiple simulations varying the T_{ice} and n_x parameters. We identified the best model fit to POLDER data, which translates into a freezing temperature T_{ice} equal to $-32°C$ instead of $-15°C$ in the standard LMDZ version. The n_x parameter is found to be equal to 1.7 instead of 6 in the standard LMDZ parametrization, which implies a flatter transition from ice to water content. New simulations have then been performed with these new values. A better agreement is found between observed and modelled short-wave cloud radiative forcing.

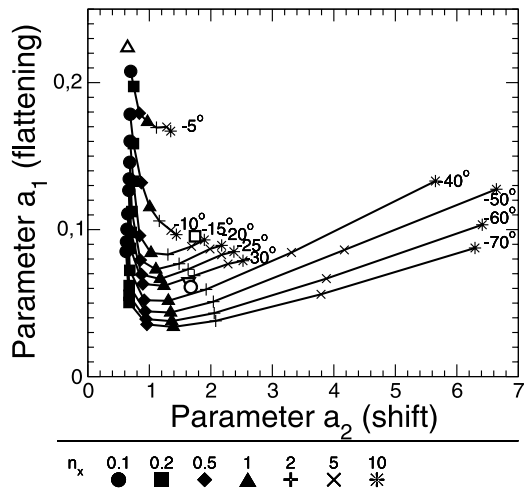

Figure 6. Scatter plot of the a_1 and a_2 parameters fitting the top-of-atmosphere cloud liquid fraction to temperature relationships. The open circle is for the POLDER observations while the other symbols depict the relationships obtained in the GCM simulations with varying T_{ice} (note that T_{ice} is expressed in °C, shown by different colors on the color version of this plot) and n_x (shown by different symbols). Note also that the up-side-down open triangle is for the simulation with the new parameters chosen for the parametrization. The open square represents simulations with the old parameters and the open triangle is for a step function at 0°C. See color version of this figure in the HTML.

[18] **Acknowledgments.** This work was supported by the CNES and Région Nord-pas de Calais. We acknowledge the Hadley Centre for providing the HADISST 1.1 SST dataset. Computer time was provided by IDRIS of the CNRS.

References

Buriez, J.-C., et al. (1997), Cloud detection and derivation of cloud properties from POLDER, *Int. J. Rem. Sens.*, *18*, 2785–2813.

Del Genio, A. D., et al. (1996), A prognostic cloud water parametrisation for global climate models, *J. Clim.*, *9*, 270–304.

Deschamp, P.-Y., et al. (1994), The POLDER mission: Instrument characteristics and scientific objectives, *IEEE Trans. Geo. Rem. Sens.*, *32*, 598–615.

Fowler, L. D., et al. (1996), Liquid and ice cloud microphysics in the CSU general circulation model. Part I: Model description and simulated microphysical processes, *J. Clim.*, *9*, 489–529.

Giraud, V., et al. (2001), Analysis of direct comparison of cloud top temperature and infrared split window signature against independant retrievals of cloud thermodynamic phase, *Geophys. Res. Lett.*, *28*, 983–986.

Goloub, P., et al. (2000), Cloud thermodynamical phase classification from the POLDER spaceborne instrument, *J. Geophys. Res.*, *105*, 14,747–14,759.

Houze, R. A. (1993), *Cloud Dynamics*, Academic Press, San Diego, 573 pp.

Kandel, R., et al. (1998), The ScaRaB earth radiation budget dataset, *Bull. Am. Meteorol. Soc.*, *79*, 765–783.

Le Treut, H., and Z.-X. Li (1991), Sensitivity of an atmospheric general circulation model to prescribed SST changes: Feedback effect associated with the simulation of cloud optical properties, *Clim. Dyn.*, *5*, 175–187.

Lohmann, U., and E. Rockner (1996), Design and performance of a new cloud microphysics scheme developed for the ECHAM general circulation model, *Clim. Dyn.*, *12*, 557–572.

Rayner, N. A., et al. (2003), Global analyses of sea surface temperature, sea ice, and night marine air temperature since the late nineteenth century, *J. Geophys. Res.*, *108*(D14), 4407, doi:10.1029/2002JD002670.

Sassen, K., and G. C. Dodd (1988), Homogeneous nucleation rate for highly supercooled cirrus cloud droplets, *J. Atmos. Sc.*, *45*, 1357–1369.

Riedi, J., et al. (2000), Global distribution of cloud top phase from POLDER/ADEOS 1, *Geophys. Res. Lett.*, *27*, 1707–1710.

Smith, R. N. (1990), A scheme for predicting layer clouds and their water content in a general circulation model, *Q. J. R. Meteorol. Soc.*, *116*, 435–460.

Tselioudis, G., et al. (1992), Global patterns of cloud optical thickness variation with temperature, *J. Clim.*, *5*, 1484–1495.

Vanbauce, C., et al. (1998), Apparent pressure derived from ADEOS-POLDER observations in the oxygen A-band over ocean, *Geophys. Res. Lett.*, *25*, 3159–3162.

Vanbauce, C., et al. (2003), Comparison of POLDER apparent and corrected oxygen pressure to ARM/MMCR cloud boundary pressures, *Geophys. Res. Lett.*, *30*(5), 1212, doi:10.1029/2002GL016449.

M. Doutriaux-Boucher, Laboratoire d'Optique Atmosphérique, UMR CNRS 8518, Université des Sciences et Technologies de Lille, 59655 Villeneuve d'Ascq Cedex, France. (marieb@loa.univ-lille1.fr)

J. Quaas, Laboratoire de Météorologie Dynamique, IPSL/CNRS, Université de Paris 6, 75252 Paris Cedex, France. (quaas@lmd.jussieu.fr)